Universiteit Leiden
The Netherlands

Weak fragment crystallizable (Fc) domain interactions drive the dynamic assembly of IgG oligomers upon antigen recognition

Strasser, J.; Jong, R.N. de; Beurskens, F.J.; Schuurman, J.; Parren, P.W.H.I.; Hinterdorfer, P.; Preiner, J.

Citation
Strasser, J., Jong, R. N. de, Beurskens, F. J., Schuurman, J., Parren, P. W. H. I., Hinterdorfer, P., & Preiner, J. (2020). Weak fragment crystallizable (Fc) domain interactions drive the dynamic assembly of IgG oligomers upon antigen recognition. *Acs Nano*, *14*(3), 2739-2750. doi:10.1021/acsnano.9b08347

Version: Publisher's Version
License: Creative Commons CC BY 4.0 license
Downloaded from: https://hdl.handle.net/1887/3182800

Note: To cite this publication please use the final published version (if applicable).

ACSNANO

www.acsnano.org

ARTICLE

Weak Fragment Crystallizable (Fc) Domain Interactions Drive the Dynamic Assembly of IgG Oligomers upon Antigen Recognition

Jürgen Strasser, Rob N. de Jong, Frank J. Beurskens, Janine Schuurman, Paul W. H. I. Parren, Peter Hinterdorfer, and Johannes Preiner*

Cite This: *ACS Nano* 2020, 14, 2739–2750

Read Online

ACCESS | Metrics & More | Article Recommendations | Supporting Information

ABSTRACT: **Activation of membrane receptors through clustering is a common mechanism found in various biological systems. Spatial proximity of receptors may be transduced across the membrane to initiate signaling pathways or alternatively be recognized by peripheral proteins or immune cells to trigger external effector functions. Here we show how specific immunoglobulin G (IgG) binding induces clustering of monomeric target molecules in lipid membranes through Fc−Fc interactions. We visualize and characterize the dynamic IgG oligomerization process and the molecular interactions involved using high-speed atomic force microscopy, single-molecule force spectroscopy, and quartz crystal microbalance experiments. We found that the Fc−Fc interaction strength is precisely tuned to be weak enough to prevent IgG oligomerization in solution at physiological titers, but enabling IgG oligomerization when Fabs additionally bind to their cognate surface epitopes, a mechanism that ultimately targets IgG-mediated effector functions such as classical complement activation to antigenic membranes.**

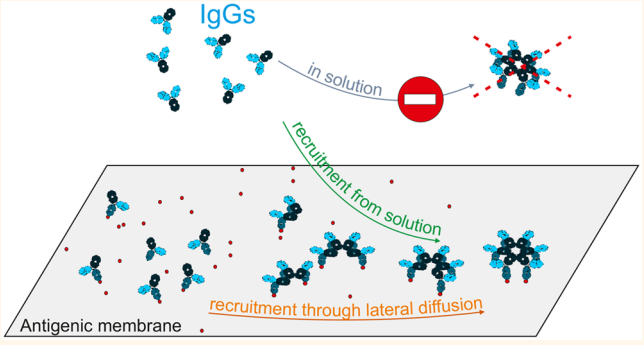

KEYWORDS: *IgG hexamers, IgG oligomerization, classical complement pathway, receptor clustering, high-speed atomic force microscopy, single-molecule force spectroscopy, quartz crystal microbalance*

Antigen-dependent immunoglobulin G (IgG) oligomerization on cells represents a recently recognized natural IgG effector function. The classical pathway of complement is initiated by the binding of factor C1 to these ordered IgG hexamers assembled at the cell surface through noncovalent Fc−Fc interactions between neighboring antibodies.[1] The fraction of IgG molecules assembled into hexamers and the potency of complement activation could be increased by specific point mutations at the Fc−Fc interface.[1,2] These mutants induced increased complement-dependent cytotoxicity (CDC) of multiple myeloma tumor cells[3] and chronic lymphocytic leukemia cells.[4] IgG oligomerization was also found to facilitate clustering of membrane receptors such as members of the tumor necrosis factor receptor (TNFR) superfamily, leading to T-cell activation, induction of apoptosis, antibody-dependent cellular cytotoxicity (ADCC), and antibody-dependent cellular phagocytosis (ADCP).[2,5−7] Recently we showed how IgG oligomerization upon antigen recognition may proceed *via* distinct mechanisms to form hexamers that recruit and tightly bind C1q, the first complement component.[8] First, epitope binding by IgGs may nucleate hexamerization in which additional IgG molecules are recruited into a growing oligomer *via* specific interactions between the Fc domains of surface-bound and soluble IgG molecules. Second, under conditions where IgG molecules bind monovalently, also lateral collisions may lead to stable IgG hexamer formation. The single-point mutant E430G[1,9] at the Fc−Fc interface was found to be more effective in inducing oligomerization than WT IgGs by generating increased populations of higher-order IgG oligomers on antigenic membranes with increased potency in complement activation and CDC.[8]

Here, we characterized the detailed molecular pathways of IgG hexamer formation and the molecular mode of action of a CDC-enhancing mutant (E430G) by a set of complementary

Received: October 22, 2019
Accepted: December 30, 2019
Published: December 30, 2019

Downloaded via LEIDEN UNIV on September 6, 2023 at 10:35:37 (UTC).
See https://pubs.acs.org/sharingguidelines for options on how to legitimately share published articles.

© 2019 American Chemical Society

https://dx.doi.org/10.1021/acsnano.9b08347
ACS Nano 2020, 14, 2739–2750

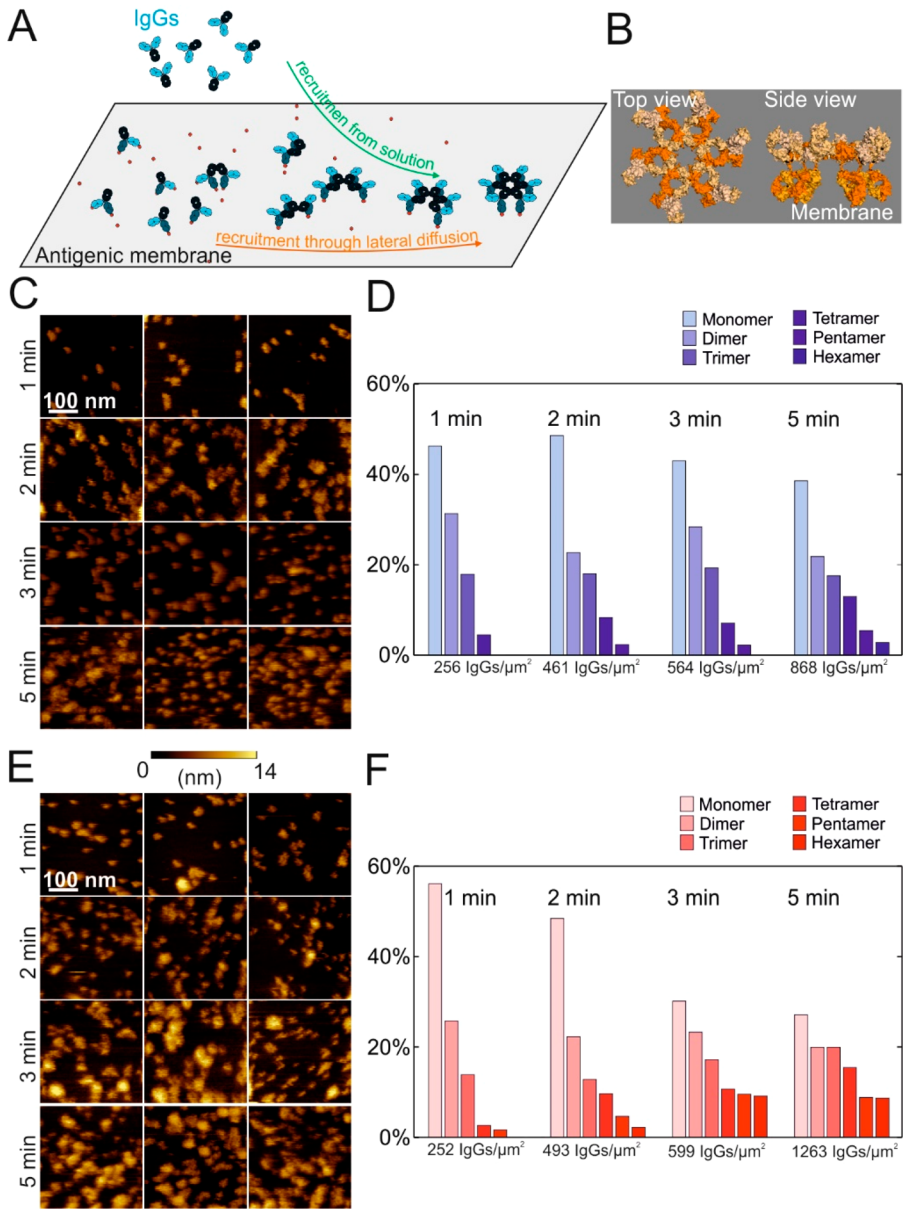

Figure 1. Formation of anti-DNP IgG oligomers on DNP-containing supported lipid bilayers (SLBs). (A) Cartoon of the IgG oligomerization pathways on antigenic membranes as determined.[8] (B) Model of the antigenic membrane bound IgG hexamer[1] based on the IgG1-b12 crystal structure.[37] (C) HS-AFM images of DNP-SLBs incubated with IgG1-DNP for 1, 2, 3, and 5 min. Increasing incubation times result in higher IgG surface densities and larger oligomeric assemblies. (D) Oligomer abundance from C. The histograms display the fraction of IgGs constituting the respective oligomer species. Absolute area densities of the respective species are given in IgGs/μm^2 and are displayed below the respective bars. Higher-order oligomers emerge with increasing incubation times, but only few hexamers are formed. (E) HS-AFM images of DNP-SLBs incubated with IgG1-DNP-E430G for 1, 2, 3, and 5 min. Larger oligomeric assemblies are more abundant than in C). (F) Oligomer abundance from E. The CDC-enhanced mutant is more efficient in forming higher-order oligomers than IgG1-DNP-WT, as hexamers are both more abundant and form more quickly.

biophysical methods. High-speed atomic force microscopy (HS-AFM), capable of directly visualizing dynamic molecular processes at submolecular spatial and millisecond time resolution under physiological conditions[10−13] enabled us to visualize the temporal progress of IgG oligomerization on antigenic lipid membranes. We further employed AFM-based single-molecule force spectroscopy (SMFS)[14] to probe specific interaction forces between individual IgGs in mechanical pulling experiments, from which we determined associated energies and chemical rate constants. Additionally, we employed quartz crystal microbalance (QCM),[15,16] in which we quantitatively studied IgG oligomerization through monitoring the resonance frequency change of an antigenic membrane covered quartz crystal resonator upon IgG binding. We developed a detailed mechanistic model of IgG oligomerization and used the experimentally determined kinetic rates to perform numerical simulations of the complex oligomerization process. Our model was validated through experimental data obtained from QCM real-time monitoring of WT- and mutant-IgG oligomerization.

RESULTS AND DISCUSSION

Time Evolution of IgG Oligomerization on Antigenic Membranes. IgG molecules interacting with cell-surface-

https://dx.doi.org/10.1021/acsnano.9b08347
ACS Nano 2020, 14, 2739−2750

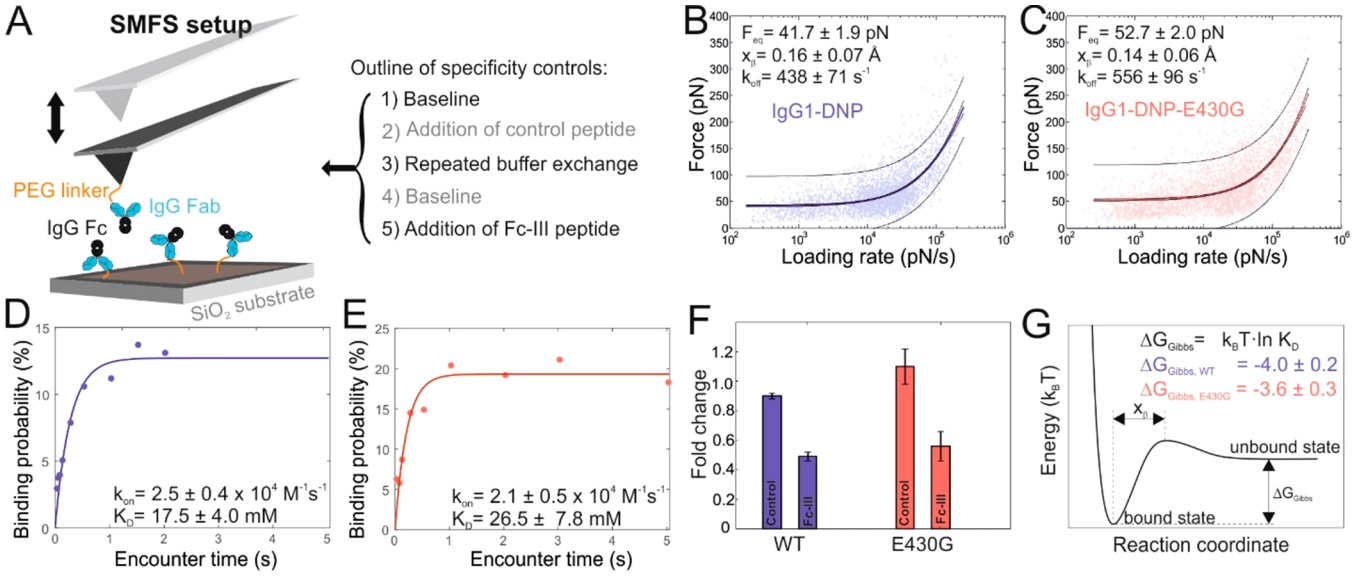

Figure 2. Single-molecule force spectroscopy (SMFS) determining energetic and kinetic parameters of Fc−Fc interactions. (A) Schematic of a SMFS experiment using the same antibody variant linked to both cantilever and SiO_2 substrate and outline of the specificity controls. (B, C) Distinctly nonlinear loading rate dependencies of homotypic Fc−Fc interaction forces for IgG1-DNP (B) and IgG1-DNP-E430G (C). The individual unbinding events as a function of their loading rate were fit using the Friddle−Noy−de Yoreo model (*cf.* Methods) (red and blue solid lines; black solid lines are 95% confidence/prediction intervals). (D, E) Binding probability as a function of the contact time for each IgG variant. The colored solid lines are the results of least-squares fits of monoexponential functions (*cf.* Methods) to determine the respective time constant, which in turn was used to find the kinetic on-rate k_{on} for each IgG. Using these values together with the k_{off} values as determined in A and B yields statistically indistinguishable K_D values of 17.5 ± 1.8 mM (IgG1-DNP) and 26.5 ± 7.8 mM (IgG1-DNP-E430G). (F) Specificity controls using the Fc binding peptide (Fc-III, *cf.* Methods) or a nonbinding peptide (Control, *cf.* Methods). The Fc-III peptide reduced the binding probability, while the control peptide did not (n = 3 for all block experiments). (G) Sketch of the free energy landscape along the Fc−Fc reaction coordinate with indicated thermodynamic parameters derived from SMFS experiments.

attached antigens may form ordered hexamers *via* specific interactions between Fc domains (Figure 1A and B). To investigate the formation of IgG oligomer populations through such Fc domain interactions in HS-AFM experiments, we used a supported lipid bilayer (SLB) containing dinitrophenyl (DNP)-labeled lipids generated from vesicle fusion as a model for an antigen/receptor-containing cell membrane.[8] Incubation of wild-type chimeric human IgG1 anti-DNP antibody (IgG1-DNP) at a fixed concentration (33 nM) for increasing time spans (1, 2, 3, and 5 min) resulted in distinct distributions of differently sized IgG oligomers on the membranes (Figure 1C). Examination of oligomer size and overall IgG surface density *via* a special HS-AFM imaging protocol (*cf.* Methods)[8] allowed us to compile quantitative oligomer distributions and overall IgG surface densities for each incubation time span. In short, molecules are scanned in a nondisrupting manner to gauge their number, height, and shape, followed by an increase in scanning force exerted by the HS-AFM cantilever tip to dissociate oligomers into their constituent IgGs. Geometric parameters and oligomer decay patterns are combined to assign each IgG assembly its oligomeric state (Figure 1D). We previously[8] found that the dominant oligomerization pathway of IgG1-DNP on DNP-SLBs is the "vertical pathway": Oligomerization nucleates from a DNP-SLB-bound IgG monomer, which grows step wisely *via* Fc−Fc-interaction-mediated recruitment of additional IgGs from solution.

With longer incubation time, the populations of higher oligomers grew, with the first hexamers appearing after 5 min. Repeating the experiment with a mutant, IgG1-DNP-E430G, with an increased ability to form oligomers, led to a shift in oligomer populations (Figure 1E and F) toward a larger fraction of higher-order oligomers, with the first hexamers already appearing after 2 min. The hexamer population was found to continuously grow over time, where the abundance of IgG1-DNP-E430G hexamers after an incubation time of 5 min was 4.5-fold higher when compared to the WT (18 *vs* 4 hexamers/μm^2), reflecting the increased CDC potency of the IgG1-DNP-E430G mutant.[8] In contrast to IgG1-DNP-E430G, a previously identified CDC-inhibiting mutant (IgG1-DNP-I253D)[1] shifts the oligomer population toward smaller oligomers (Figure S1), demonstrating the specificity and sensitivity of IgG1 oligomerization to mutations at the Fc−Fc interface.

Homotypic Fc Interactions Are Weak. To answer the question whether the increased oligomerization propensity of the CDC-enhancing mutant IgG1-DNP-E430G on epitope-carrying SLBs is related to a mutation-induced strengthening of the Fc−Fc interactions, we performed SMFS experiments.[14,17] Energies and chemical rate constants involved in IgG homotypic binding were determined by probing the dissociation forces between individual IgGs in AFM-based mechanical pulling experiments (Figure 2). Due to the poly(ethylene glycol) (PEG) linkers spacing the antibodies from the AFM cantilever tip and the SiO_2 substrate surface, respectively, the binding partners are free to rotate in three dimensions, mimicking the situation in solution.[18,19] Force curves were recorded at a wide range of loading rates, revealing distinct nonlinear force spectra (Figure 2B and C) for both IgG1-DNP-WT and the CDC-enhanced variant (IgG1-DNP-E430G). Analysis according to the Friddle−Noy−de Yero model[17] revealed dissociation rates $k_{off,WT}$ = 438 ± 71 s^{-1} and $k_{off,E430G}$ = 556 ± 96 s^{-1} for the homotypic Fc−Fc interactions. The respective association rates (k_{on}) were determined from the dependency of the binding probability (*i.e.*, the probability

https://dx.doi.org/10.1021/acsnano.9b08347
ACS Nano 2020, 14, 2739−2750

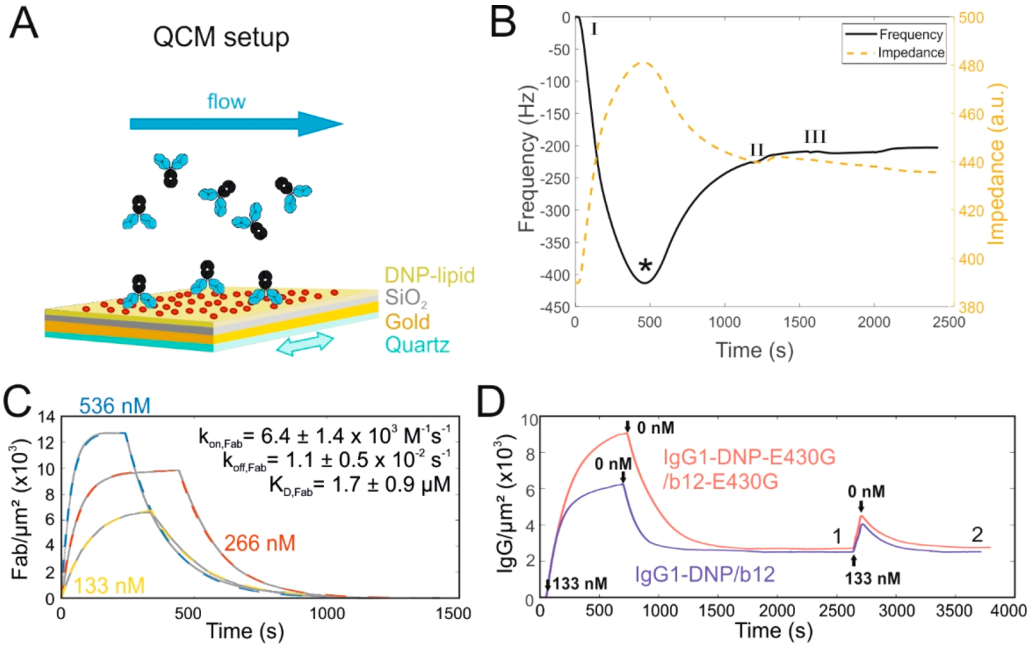

Figure 3. Quartz crystal microbalance (QCM) of antibody variants on DNP-SLBs. (A) Schematic of a QCM experiment with IgGs in the running buffer over a DNP-SLB prepared on the SiO_2-coated gold electrode of an oscillating quartz crystal. (B) Preparation of DNP-SLBs on QCM senor chips *via* liposome fusion and a routine test to ensure complete lipid coverage. Buffer #1 was used for equilibration before introducing the lipid suspension. At (I) 200 μg/mL of DNP-labeled liposomes were injected into the QCM liquid cell. The liposomes first associated with the SiO_2-coated QCM crystal (until *) and then started to fuse. The release of their liquid content (*i.e.*, loss of mass) during fusion reduced the frequency shift (trace after *). At (II), the running buffer was changed to buffer #1. The lipid fusion continued for a few minutes. Then, at (III), the running buffer was changed to 133 nM of the control antibody IgG1-b12. No association was observed, indicating that the lipids indeed covered the entirety of the QCM crystal. This sequence was routinely performed before every measurement. The impedance curve consistently mirrors the frequency changes reflecting the energy dissipation due to the associated mass. (C) QCM sensorgrams (gray solid lines; converted to Fab/μm^2) recorded at different IgG1-DNP-Fab concentrations (as indicated) are best fit by a 1:1 Langmuir interaction model (dashed lines) with kinetic rates as indicated. (D) QCM sensorgrams obtained for functionally monovalent bsIgGs at 133 nM on DNP-SLBs. A short additional association phase of ~70 s does not increase the overall amount of stably bound IgGs at the end of the experiment (compare levels indicated by numbers 1 and 2), suggesting that the IgGs that remain stably bound after the first injection (1) do not interact with additional IgGs provided in solution.

to observe a dissociation event in a given set of force curves) on the encounter time of tip- and surface-bound IgGs during which a complex can be formed.[20] Varying this time span and evaluating the corresponding binding probabilities yields typical saturation curves (Figure 2D and E), resulting in $k_{on,WT} = (2.5 \pm 0.4) \times 10^4$ M^{-1} s^{-1} and $k_{on,E430G} = (2.1 \pm 0.5) \times 10^4$ M^{-1} s^{-1}. The specificity of these interactions was confirmed by blocking experiments involving a peptide termed Fc-III, which specifically interacts with the Fc−Fc binding interface and thereby inhibits Fc-binding and complement activation[1,21] (Figure 2F). With $K_D = k_{off}/k_{on}$ we obtained values for the equilibrium dissociation constants, $K_{D,WT} = 17.5 \pm 4.0$ mM and $K_{D,E430G} = 26.5 \pm 7.8$ mM, respectively (Figure 2G). This clearly suggests that considerable oligomer formation in solution is effectively precluded at physiological titers (~40−50 μM total IgG1)[22,23] and rationalizes why native mass spectrometry experiments solely detected monomers (and no higher oligomers) of both WT and E430G IgG1 in solution.[9]

Accordingly, we found that incubation of a mixture of DNP-specific IgG1-DNP and irrelevant isotype control antibody IgG1-b12 at 300-fold excess (20 nM vs 6 μM) on DNP-labeled SLBs did not affect the resulting IgG distribution and surface density (Figure S2), suggesting that the Fc−Fc interaction alone is not sufficient to incorporate an IgG into an oligomer. Moreover, the K_D values determined for homotypic Fc−Fc interactions of WT and E430G mutant IgG1 are statistically not distinguishable so that a mutation-induced stabilization of the Fc−Fc interaction of IgG1-DNP-E430G that could possibly cause increased oligomerization propensity can be ruled out. The mutation-related oligomerization enhancement observed with HS-AFM (Figure 1) must therefore be induced upon binding to antigenic surfaces.

Weak Fc Interactions Induce IgG Oligomerization upon Antigen Binding. To gain further insight into the interactions and rate constants governing IgG oligomerization on antigenic surfaces, we performed a series of quartz crystal microbalance experiments[15,16] (Figure 3A) utilizing the same DNP-SLBs (Figure 3B) used in HS-AFM. Monitoring the change of the oscillation frequency of the DNP-SLB-covered SiO_2-coated quartz crystal, which is proportional to the change in bound mass, yields characteristic binding curves of IgGs or Fab fragments interacting with DNP-SLBs. To exclude valency contributions, we compared the binding of functionally monovalent bispecific (bs)IgGs. These bsIgG molecules consist of two distinct binding arms, one specific for the DNP antigen and the other with an, for this experiment, innocuous specificity (bsIgG1-DNP/b12, bsIgG1-DNP-E430G/b12-E430G). Importantly, the generation of bsIgG1 variants does not impact on the Fc-glycosylation, so that a potential glycan-related alteration of the homotypic Fc−Fc interactions (with respect to the monospecific WT IgG1-

https://dx.doi.org/10.1021/acsnano.9b08347
ACS Nano 2020, 14, 2739−2750

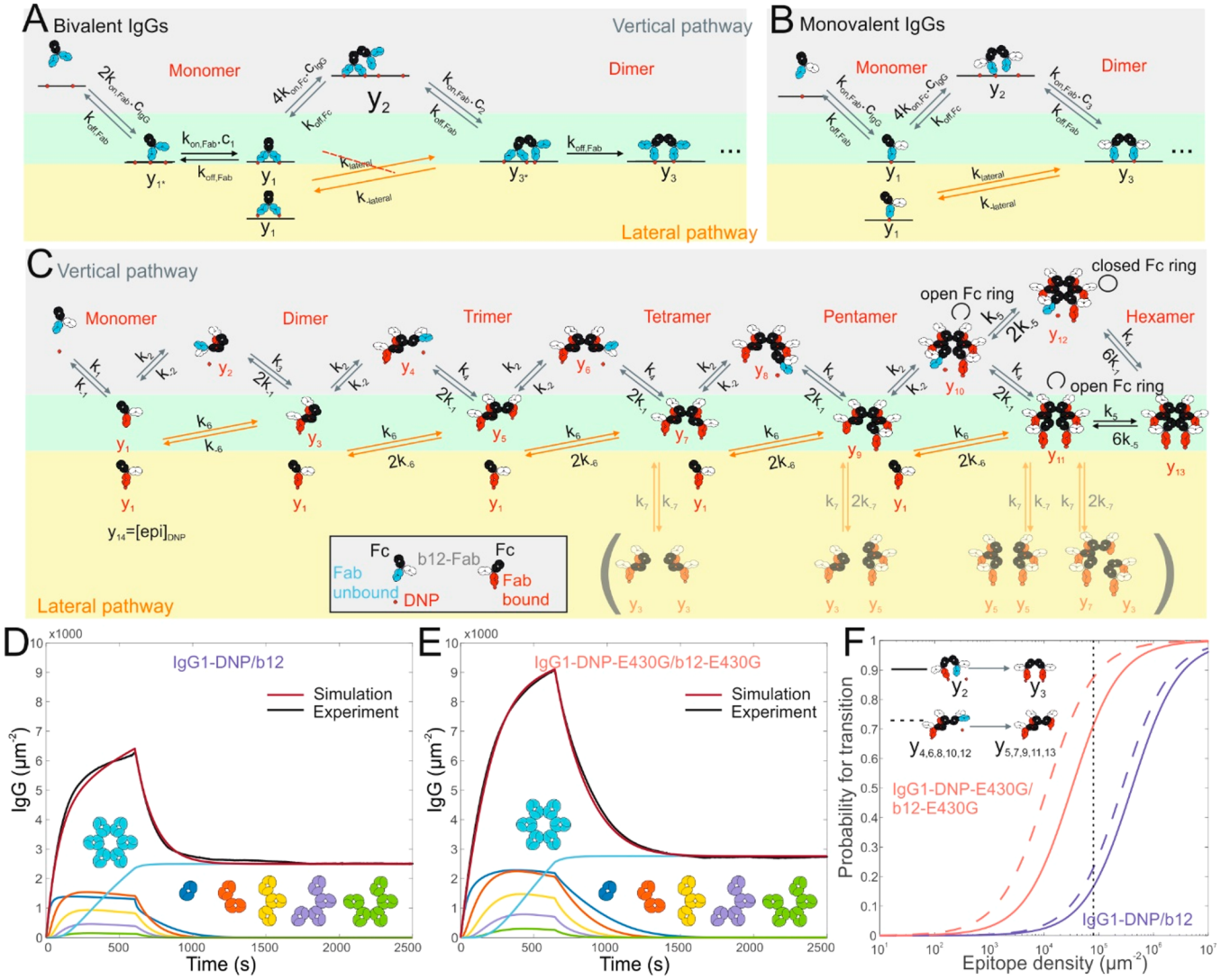

Figure 4. Mechanism of IgG oligomerization. (A) Dynamic model of IgG oligomerization at high epitope density (single IgGs predominantly in the bivalently bound state). IgGs (y_1) may serve as nucleation sites for oligomerization through recruitment from solution (y_2 to y_{3*} vertical pathway), whereas lateral collisions (lateral pathway) between bivalently bound IgGs do not significantly contribute (y_1 directly to y_3), likely because bivalent attachment of both potential partners sterically precludes Fc−Fc interactions. (B) Monovalently bound IgGs have access to an additional pathway. After initial attachment (state y_1), oligomerization continues either *via* recruitment from solution (state y_2) or *via* lateral collisions ($y_1 \times y_1$), leading to dimers (state y_3) and through repetition of either pathway to higher oligomers. (C) Oligomerization scheme for IgGs that are predominantly monovalently bound to surface epitopes. These could be either functionally monovalent IgGs at arbitrary epitope densities or functionally bivalent IgGs at low epitope densities where the probability for a transition from $y_{1*} \rightarrow y_1$, $P_{y_{1*} \rightarrow y_1} \approx 0$ (eq 4), can be neglected. In this case, two different oligomerization pathways exist, recruitment from solution (gray arrows; vertical pathway) or oligomerization through lateral collisions (orange arrows; lateral pathway). After initial attachment (state y_1), oligomerization continues either *via* recruitment from solution (state y_2) or *via* lateral collisions ($y_1 \times y_1$), leading to dimers (state y_3) and through repetition of either pathway to higher oligomers. (D, E) Comparison of simulated and experimental QCM sensorgrams of functionally monovalent IgGs binding to DNP-SLBs. 133 nM bsIgG1-DNP/b12 on a 5 mol % DNP SLB (D) and 133 nM bsIgG1-DNP-E430G/b12-E430G on a 5 mol % DNP SLB (E). Dark blue, red, yellow, purple, green, and light blue lines represent the contributions of IgG monomers, dimers, trimers, tetramers, pentamers, and hexamers to the simulated sensorgrams (red lines), respectively. (F) Transition probabilities as a function of epitope density [epi] calculated from $P_i = \frac{k_i[\text{epi}]}{k_{\text{off,Fc}} + k_i[\text{epi}]}$ using the values for k_3 and k_4 obtained from D and E (Table 1). The vertical dashed line indicates the initial epitope density used in our model system.

DNP) can be ruled out.[24] In addition, we also assessed the binding of monovalent Fab fragments (IgG1-DNP-Fab). The IgG1-DNP-Fab bound reversibly to the SLBs and are nicely fitted with a 1:1 Langmuir binding model (Figure 3C) with association rate $k_{\text{on,Fab}} = (6.4 \pm 1.4) \times 10^3$ M^{-1} s^{-1} and dissociation rate $k_{\text{off,Fab}} = (1.1 \pm 0.5) \times 10^{-2}$ s^{-1}, resulting in $K_{\text{D,Fab}} = 1.7 \pm 0.9$ μM.

In contrast, the binding behavior of the two monovalent bsIgGs (Figure 3D) that contain an Fc portion was strikingly different: Equilibrium was not reached (within association times of up to 120 min used in these experiments) and, most importantly, a considerable amount of molecules remained stably bound throughout the dissociation phase. The association phase started exponentially and subsequently transitioned into a linear regime, likely representing the

https://dx.doi.org/10.1021/acsnano.9b08347
ACS Nano 2020, 14, 2739−2750

signature of oligomerization through Fc−Fc interactions. The sensorgrams of both bsIgGs variants share similar overall features, but the exponential phase in the beginning of the experiment and the amount of stably bound molecules at the end of the experiment were more pronounced for bsIgG1-DNP-E430G/b12-E430G. Apparently, the Fc interactions of the two monovalent bsIgGs led to oligomer-induced "quasi-multivalent" attachment to the antigens. This was already demonstrated for the very same monovalent bsIgGs in HS-AFM experiments,[8] which, in contrast to the observation with Fab fragments, precluded complete dissociation of monovalent bsIgG oligomers.

Kinetics of the IgG1 Oligomerization Process. Based on the determined kinetic rates and estimates of the local Fab concentrations within the respective IgG oligomers (*cf.* Methods) we can now map out the IgG oligomerization process in detail. Depending on the affinity of the monovalent epitope−paratope interaction and the epitope density/accessibility for bivalent binding, single IgGs are predominantly either bivalently (IgG1-DNP) or monovalently (bispecific IgG1-DNP/b12) attached to surface epitopes. A model of this process is shown in Figure 4. During nucleation (Figure 4A), an IgG from solution binds monovalently to a surface epitope (state y_{1*}), followed by almost immediate bivalent attachment (state y_1) as $k_{off,Fab}$ (1.1×10^{-2} s^{-1}) ≪ $k_{on,Fab} \times c_1$ = 91.5 s^{-1} (c_1 = 14.3 mM, for our SLBs, *cf.* Methods, eqs 3 and 4). Additional IgGs are recruited through Fc−Fc interactions (2 × 2 possible realizations, $4k_{on,Fc}$) to the vicinity of the membrane (state y_2). The corresponding local epitope/paratope concentration c_2 (22.3 mM, *cf.* Methods) enables the formation ($k_{on,Fab} \times c_2$ = 142.7 s^{-1}) of an epitope−paratope bond (success rate ~18%, eq 4) before the Fc−Fc interaction dissociates, resulting in a "tripod" arrangement (state y_{3*}). After the release of one epitope−Fab bond ($2k_{off,Fab}$), an IgG dimer is realized, provided that the distance of the remaining epitope−Fab bonds can adapt to the new situation (states y_{3*} and y_3 likely require different epitope distances and the transition in between these states requires the epitopes themselves to be mobile). In fact, IgG hexamer formation could not be observed on spatially fixed hexameric epitope patterns[25] likely because state y_{3*} cannot be realized on such an epitope geometry, and oligomerization might even further be hindered as soon as other epitope pairs within the hexagonal arrangement are occupied by an additional IgG. However, in the case of mobile antigens, states y_{3*} and y_3 may both be realized, and oligomerization continues *via* further recruitment of IgGs out of solution. When IgGs are predominantly monovalently bound (Figure 4B), oligomerization may occur *via* both pathways, *i.e.*, recruitment from solution (vertical) and 2D collisions (lateral). Compared to the weak Fc−Fc interaction in solution, surface-bound IgG oligomers are additionally stabilized by the epitope−paratope interaction. In case of dissociation of one of these two bonds at the open ends of an IgG oligomer (*i.e.*, dimers to pentamers; IgGs that have only one direct neighbor within an oligomer), the high effective concentration c_{eff} leads to fast rebinding, which can be expressed in an overall equilibrium dissociation constant according to[26]

$$K_{D,Olig} = K_{D,Fab} K_{D,Fc} \frac{1}{c_{eff}} \quad (1)$$

Estimation of c_{eff} through the volume, in which an unbound Fab/Fc may be confined (modeled as a half-sphere with r = 6 nm; *cf.* methods), yields c_{eff} = 33.5 mM, which together with the experimentally determined $K_{D,Fab}$ and $K_{D,Fc}$ results in an affinity of $K_{D,Olig}$ = 889 nM for an IgG to an SLB-bound IgG oligomer. Thanks to the additional epitope−paratope interactions, the affinity for oligomerization upon antigen binding in our system is 5 orders of magnitude higher than in solution, a mechanism that targets IgG effector functions such as the classical complement pathway to antigenic membranes, while preventing its unwanted activation in serum.

Mechanistic Model of the IgG Oligomerization Process. On the basis of this basic concept, we have developed a complete kinetic scheme depicting the combination of pathways for functionally monovalent IgGs (or predominantly monovalently epitope-bound IgGs) to complete hexamerization (Figure 4C). From this scheme we deduced the corresponding system of rate equations (Methods) that determines the time course of the respective surface populations of different IgG oligomer configurations (y_1−y_{13}), the surface density of available epitopes (y_{14}), and the local concentration of IgGs close the surface (y_{15})[27] for a given IgG concentration in the bulk solution, C_{IgG}. For the simulations (Figure 4D; Methods; Table 1) we have neglected more complex (thus less probable) processes like the splitting/association of higher oligomers as depicted in the lower part of the scheme (brackets). The simulations reasonably reproduce the experimental QCM sensorgrams (Figure 4D and E) and additionally reveal the contributions of different oligomer species, suggesting that the linear increase found instead of an equilibrium during the association phase is caused by the growing fraction of hexamers that are allosterically stabilized by their closed Fc ring. Accordingly, the simulation suggests that the only oligomer species that remain stably bound to DNP-

Table 1. Parameters Used for Simulating the Experimental QCM Sensorgrams of Monovalent IgGs

fixed parameters	WT	E430G
$k_1 = k_{on,Fab}$	6.4×10^3 M^{-1} s^{-1}	
$k_{-1} = k_{off,Fab}$	1.1×10^{-2} s^{-1}	
$k_2 = 4k_{on,Fc}$ [a]	9.9×10^4 M^{-1} s^{-1}	8.4×10^4 M^{-1} s^{-1}
$k_{-2} = k_{off,Fc}$	438 s^{-1}	556 s^{-1}
floating parameters		
$\alpha = k_3[epi]/k_{off,Fc}$	0.2	2.5
$\beta = k_4[epi]/k_{off,Fc}$	0.3	7.0
$\gamma = k_5/k_{on,Fc}$	>250 mM[b]	
k_{-5}[c]	0 s^{-1}	
k_6[d]	1.3×10^{-5} $\mu m^2 s^{-1}$	0.3×10^{-5} $\mu m^2 s^{-1}$
k_{-6}[d]	1.3×10^{-2} s^{-1}	
k_{tr}[e]	2×10^9 s^{-1}	0.9×10^9 s^{-1}

[a]There are four different realizations of Fc−Fc interactions between an oligomer on the surface and an IgG in solution. [b]The min. value of 250 mM corresponds to a max. distance between Fc interaction sites in the gap of the open Fc ring (when treated as a sphere) of ~2.3 nm. [c]k_{-5} = 0 s^{-1} reflects the great stability of the hexameric Fc ring independent of the IgG variant. [d]k_6 on the order of 10^{-5} μm^2 s^{-1} (thus $k_6 y_i y_j$ is approximately on the order of 1 μm^{-2} s^{-1}) and k_{-6} on the order of 10^{-2} correspond to a low effective lateral oligomerization/dissociation rate, which can both be attributed to the slow lateral mobility of antigens in our gel-phase SLB. This is also in accordance with our previous findings that the "vertical" oligomerization pathway dominates the overall process in our model system. [e]Values for mass transport limitation are in the typical range for such a process reported in the literature.[27]

https://dx.doi.org/10.1021/acsnano.9b08347
ACS Nano 2020, 14, 2739−2750

SLBs at the end of the experiment are hexamers, which is supported by the fact that an additional, subsequent (~70 s) association phase (Figure 3B) does not contribute to the overall level of stably bound IgGs at the end of the experiment. This is because the hexamers do not interact with newly supplied IgGs (as all potential Fc binding sites are occupied), and the duration of these subsequent experiments is simply too short for hexamers to be formed starting from the very beginning, *i.e.*, with single IgGs as nucleation sites.

We can estimate the overall equilibrium dissociation constant for an IgG bound in an IgG hexamer by extending eq 1 to three interactions,[26] accounting for two Fc−Fc interactions and one epitope−paratope interaction. The corresponding equation then reads

$$K_{D,Hex} = K_{D,Fab}\left(\frac{K_{D,Fc}}{\tilde{c}_{eff}}\right)^2 \quad (2)$$

Through the additional confinement (two neighboring IgGs) it follows that $\tilde{c}_{eff} > c_{eff}$, and thus $K_{D,Hex} < K_{D,\,Olig}$, *i.e.*, that through closing of the hexameric Fc ring, hexamers are allosterically stabilized. Using the minimal value for $\tilde{c}_{eff}$ obtained from the simulation (γ = 250 mM, Table 1), it follows that $K_{D,Hex}$ < 0.8 pM. Rates k_3 and k_4 (Table 1) were used to calculate the respective effective concentrations in states y_2 ($c_3 = k_3/k_{on,Fab}$) and y_4, y_6, *etc.* ($c_4 = k_4/k_{on,Fab}$) and to validate their plausibility through comparison to c_{eff} estimated above (eq 1). We retrieved $c_{3,WT}$ = 13.7 mM, $c_{3,E430G}$ = 21.7 mM and $c_{4,WT}$ = 20.5 mM, $c_{4,E430G}$ = 60.1 mM, which are all within a factor 0.5 to 2 of c_{eff}, as estimated from pure geometrical considerations. It is thus only the confinement to the respective binding sites within an oligomer, amplified through the combination of Fc−Fc and epitope−paratope interactions, that leads to such high local concentrations, thereby driving IgG oligomerization. Considering that in state y_2 the unbound Fab may explore a larger volume than in y_4, y_6, *etc.*, it is further consistent that the corresponding effective concentrations are lower. The E430G mutant is more efficient in recruiting IgGs from solution than the WT, as already suggested by our HS-AFM experiments (Figure 1), which is caused by the increased effective concentrations in the respective states ($c_{3,E430G} > c_{3,WT}$ and $c_{4,E430G} > c_{4,WT}$). Consequently, the probabilities (Figure 4F) for configurations y_2/y_4 (Figure 4C) to transit into y_3/y_5 with rates k_3/k_4 instead of dissociating back into y_1/y_3 (rate $k_{-2} = k_{off,Fc}$) are strongly increased for the E430G mutant (71.4/87.5%; values were calculated for the total epitope density used in our model system) when compared to the WT (16.7/23.1%) through a wide range of different epitope densities. The increased oligomerization propensity of the E430G mutant may thus be attributed to either a further constraint of the accessible volume for the free Fab and/or an increased accessibility of surface epitopes (*cf.* eq 3) in states y_2, y_4, y_6, *etc.* In fact the E430G point mutation removes a salt bridge that stabilizes the CH_2-CH_3 interface packing, restraining the domain motility of Fc fragments in the WT,[2] which may indeed affect the overall flexibility of the complex and thus the effective volume and the surface epitope accessibility in these configurations.

CONCLUSIONS

We uncovered the molecular mechanism that ultimately targets IgG effector functions to antigenic membranes, thus providing opportunities for guiding cell surface receptors into functional clusters. The low, mM affinity of homotypic Fc−Fc interactions thereby prevents IgG oligomerization and thus target-independent activation of effector functions in solution at physiological titers. However, upon IgG attachment to target surfaces, the weak Fc−Fc interactions enable two different oligomerization pathways, which, depending on the epitope density and the resulting preferential monovalent or bivalent binding state of the IgGs, lead to membrane-bound IgG oligomers. Importantly, oligomerization requires the presence of a certain antigen and does not support the incorporation of target-irrelevant IgGs into oligomers.

Unlike monovalently bound IgGs, IgGs bivalently attached to multimeric or preoligomerized antigens or receptors are unable to oligomerize through lateral diffusion-driven encounters. Application of functionally monovalent IgGs in such situations instead, however, enables this additional pathway.[1,8] Specially designed IgG mutants such as E430G further allow for the optimization of specific steps within these pathways. In this way, antibodies activate the classical complement system[1,8] or cluster and consequently activate low-density antigens, such as TNFR.[5,6] We characterized the involved molecular interactions and developed and validated a detailed mechanistic model of IgG oligomerization on antigenic surfaces, which may serve as a framework for immunotherapy optimization.

METHODS

DNP-Labeled Liposomes. DNP-labeled liposomes consisting of 1,2-dipalmitoyl-*sn*-glycero-3-phosphocholine (DPPC), 1,2-dipalmitoyl-*sn*-glycero-3-phosphoethanolamine (DPPE), and 1,2-dipalmitoyl-*sn*-glycero-3-phosphoethanolamine-*N*-[6-[(2,4-dinitrophenyl)amino]-hexanoyl] (DNP-cap-DPPE) were used to generate supported lipid bilayers on mica and SiO_2 substrates. The lipids were purchased from Avanti Polar Lipids, mixed at a ratio of DPPC:DPPE:DNP-cap-DPPE = 90:5:5 (molar ratio), and dissolved in a 2:1 mixture of chloroform and methanol. The solvents were rotary-evaporated for 30 min, and the lipids were again dissolved in chloroform, which was then rotary-evaporated for 30 min. Drying was completed at a high vacuum pump for 2 h. The lipids were dissolved in 500 μL of Milli-Q H_2O while immersed in a water bath at 60 °C, flooded with argon, and sonicated for 3 min at 60 °C to create small unilamellar vesicles. These were diluted to 2 mg/mL using buffer #1 (10 mM HEPES, 150 mM NaCl, 2 mM $CaCl_2$, pH 7.4) and frozen for storage using liquid N_2.

High-Speed Atomic Force Microscopy. HS-AFM (RIBM, Japan) was conducted in tapping mode at RT (room temperature, 25 °C) in liquid, with free amplitudes of 1.5−2.5 nm and amplitude set points larger than 90%. Silicon nitride cantilevers with electron-beam-deposited tips (USC-F1.2-k0.15, Nanoworld AG), nominal spring constants of 0.15 N m^{-1}, resonance frequencies around 500 kHz, and a quality factor of approximately 2 in liquids were used. Imaging was performed in buffer #1, unless noted otherwise. All IgGs were diluted and incubated in buffer #1.

DNP-labeled supported lipid bilayers (DNP-SLBs) for HS-AFM were prepared on muscovite mica. The liposomes were incubated on the freshly cleaved surface (350 μg mL^{-1} in buffer #1), placed in a humidity chamber to prevent evaporation, and heated to 60 °C for 30 min. Then the temperature was gradually cooled to RT within 30 min, followed by exchanging the solution with buffer #1. After 10 min of equilibration at RT and 15 more buffer exchanges, the SLB was ready for imaging. In order to passivate any exposed mica, SLBs were incubated with 333 nM IgG1-b12 (irrelevant human IgG1 control antibody against HIV-1 gp120)[28] for 10 min before the molecules of interest were added.

IgG Oligomer Statistics on DNP-SLBs. IgG oligomer distributions were then obtained by incubating DNP-SLBs with 33.3 nM of the respective IgG variant for 1, 2, 3, or 5 min and analyzed in a two-step process: Individual particle dimensions were determined by HS-

https://dx.doi.org/10.1021/acsnano.9b08347
ACS Nano 2020, 14, 2739−2750

AFM, and the respective oligomeric states were further confirmed by observing their decay pattern determined in subsequent forced dissociation experiments as described.[8]

Single Molecule Force Spectroscopy. SMFS measurements were conducted on a PICO SPM LE 5100 AFM (Keysight, formerly Agilent, USA) using a small scanner (N9520A), fitted with a contact mode nose, and the software PicoView 1.10. Measurements were performed in buffer #1 at pH 7.4. Commercial cantilever chips with nominal spring constants of 10−20 pN/nm (model MSCT, Bruker, USA) were used. Acetal-PEG$_{18}$-NHS linkers were synthesized and provided by Hermann J. Gruber (Institute of Biophysics, University of Linz, Austria). SiO_2 wafers served as substrate. Cantilever spring constants were determined using the Keysight Thermal K package. The resulting values varied between 10.3 and 13.7 pN/nm.

Square silicon substrates were cleaned *via* ultrasonication in ethanol for 10 min prior to functionalization. All cantilevers and silicon chips were washed in $CHCl_3$, dried in a stream of N_2, and oxidized using air plasma (4 min at 40 W for cantilevers; 3 min at 80 W for solid substrates). Functionalization of both AFM cantilevers and silicon substrates was performed as described.[29] Briefly, the inert silicon oxide was activated *via* amino functionalization using aminopropyltriethoxysilane (APTES), followed by the attachment of heterobifunctional PEG cross-linkers. Finally, tips/substrates were conjugated with the respective IgGs to the free end of the PEG cross-linker.

For determination of the dissociation rate constant $k_{off,Fc}$, the pulling velocity was varied in 11 steps between 50 and 16 000 nm/s, with no data set containing less than 500 curves. The probed spot on the sample surface was periodically changed during the measurement. The total encounter time was kept constant between loading rates. Data analysis for SMFS was performed using a MATLAB (Mathworks) routine developed in-house. To fit the resulting force spectra, we used the analytical approximation of the Friddle−Noy−de Yoreo model[17] where the mean rupture force as a function of the force loading rate r is given by $F(r) = F_{eq} + F_\beta \ln\left[1 + \frac{r \exp(-\gamma)}{k_{off}(F_{eq})F_\beta}\right]$, and $k_{off}(F) = k_{off,Fc} \exp\left[\beta\left(Fx_\beta - \frac{1}{2}k_{eff}x_\beta^2\right)\right]$, with $\gamma = 0.5772$ being Euler's constant, F_{eq} being the equilibrium force, F_β given by $F_\beta = k_BT/x_\beta$, x_β being the distance between the bound state and the transition state, and k_{eff} being the effective spring constant of the force transducer system.

Association rate constants $k_{on,Fc}$ were determined as described.[20] Briefly, nine encounter times between 30 and 5050 ms were chosen, and the resulting binding probability p_b (measured at a pulling velocity of 400 nm/s) was determined from 1000 curves at each setting. Plots of p_b over encounter time were fitted by $p_b = p_{max}\left[1 - \exp\left(-\frac{t}{\tau}\right)\right]$, with p_{max} being the maximum observable binding probability, t being the encounter time, and τ being the characteristic time constant of association. Estimation of k_{on} according to $k_{on} = (\tau c_{eff})^{-1}$ requires knowledge of the effective concentration c_{eff}, which describes the number of binding partners (IgGs) within the effective volume V_{eff} accessible for free equilibrium interaction. V_{eff} can be described as a half-sphere with radius r_{eff}, which is given by the sum of the equilibrium cross-linker length (6 nm) and the average distance from the cross-linker anchoring point on the IgG to the Fc−Fc interface (8 nm). For the interaction of two IgGs there are four different realizations of Fc−Fc interactions (both IgGs have two Fc−Fc interfaces), so that c_{eff} finally reads $c_{eff} = \frac{4p_{max}N_A}{V_{eff}}$, with N_A being Avogadro's constant.

Specificity controls were done by introducing 16.7 μM of the Fc−Fc interface binding Fc-III peptide[1,21] or 16.7 μM of a control peptide[1] into the AFM liquid cell while recording force curves (for 45 min; $n > 2500$ curves for each control). A set of 1000 force curves was recorded (400 nm/s) prior to the respective specificity control experiment, and the fold-change of binding probability with respect to the control was determined.

Quartz Crystal Microbalance. All QCM experiments were done using a two-part liquid chamber (model LCS01,[16] Johannes Kepler University Linz, Austria) connected to a Keysight E4990 impedance analyzer (Keysight Technologies, Santa Rosa, CA, USA). A constant flow rate of 50 μL min^{-1} was provided by a programmable syringe pump (NE-1000, New Era Pump Systems Inc., New York, NY, USA). AT-cut SiO_2-coated quartz crystals with a diameter of 13.7 mm (working surface area of 20.47 mm^2) and a resonance frequency of 9.995 MHz were used (ICM, Oklahoma City, OK, USA). All sensorgrams were recorded on the fifth harmonic frequency and normalized accordingly.[16] Before each set of experiments, the SiO_2-coated crystals were cleaned by immersion in dilute sodium dodecylsulfate (SDS) overnight, followed by rinsing with Milli-Q H_2O and immersion in Milli-Q H_2O for 20 min. The chips were dried in a gentle stream of N_2 and oxidized using air plasma (3 min at 80 W), after which they were mounted in the measurement chamber. The sensor surface was further cleaned by a flow of 10 mM SDS at 150 μL min^{-1} for 3 min, followed by Milli-Q H_2O at 150 μL min^{-1} for 5 min directly before the measurement. Finally, IgG-free buffer was injected for equilibration at 50 μL min^{-1} (approximately 1 h). All subsequent injections were performed at 50 μL min^{-1}. Between experiments on the same day, the chip was regenerated by 10 mM SDS at 150 μL/min for 5 min, followed by Milli-Q H_2O at 150 μL min^{-1} for 5 min and finally buffer #1 for equilibration at 50 μL min^{-1} (at least 30 min). To generate DNP-SLBs on QCM chips, the DPPC:DPPE:DNP-cap-DPPE liposome stock solution was heated to 60 °C for 30 min and slowly cooled down to RT within 30 min. The solution was ready for injection after dilution to 200 μg/mL with buffer #1. DNP-SLB formation was typically complete after 30 min at 50 μL min^{-1}, after which the flow medium was changed to buffer #1 for 10 min of equilibration. Finally, an injection of 133 nM IgG1-b12 was performed prior to each experiment to check for unspecific binding and to ensure that the entire working surface was covered by the DNP-SLB.

Conversion of QCM Sensorgrams. Raw sensorgrams (in Hz *vs* time) were converted to molecule densities on the QCM chip (molecules/μm^2 *vs* time) by determining the bound mass according to the Sauerbrey equation,[30] which relates the change in resonance frequency Δf of a quartz crystal oscillating in thickness shear mode to the mass adsorbed on its surface Δm by the relation $\Delta f = \frac{2f_0^2}{\sqrt{\rho_q \mu_q}}\frac{\Delta m}{A}$. Here f_0 is the fundamental resonance frequency, and ρ_q and μ_q are the crystal density (2.648 g cm^{-3}) and its shear modulus (2.947 × 10^{11} g cm^{-1} s^2), respectively. The resulting masses were corrected for the effect of trapped water according to Höök *et al.*[31] Determination of molecule densities further requires the effective surface area of the DNP-SLBs, which may exceed the actual working surface area of the QCM chip due to residual, only partially fused (and thus nonflat) vesicles. We corrected the active surface area accordingly by comparing the theoretical mass of a flat DNP-SLB covering the working surface (average molecular weight of 729.3 Da for DPPC:DPPE = 9:1; headgroup area of 0.626 nm^2,[32] 0.5 nm buffer layer between SiO_2 and DNP-SLB) to the actual observed mass, and modeling the excess as buffer-filled half-spheres with a diameter of ∼35 nm (determined by HS-AFM imaging).

Determination of Kinetic Rates from QCM Sensorgrams. Kinetic rates were obtained by fitting the solution of a 1:1 Langmuir interaction model simultaneously to the association and dissociation phases of QCM sensorgrams using in-house MATLAB (Mathwork) routines.

Construction, Expression, and Purification of Antibody Variants. The antibodies used in this work were chimeric anti-DNP mAb G2a2 consisting of the mouse variable domain of antibody G2a2[33] fused to the human IgG1 and kappa light chain constant regions,[34] and the human control antibody IgG1-b12 (directed against anti-gp120 of HIV-1[28]). For generation of Fc:Fc interaction-enhanced antibodies, the E430G mutation was introduced into wild-type or functionally monovalent bispecific antibodies.[1] bsIgGs were produced by introduction of a K409R mutation in one antibody and an F405L mutation in the other, which enabled the production of

https://dx.doi.org/10.1021/acsnano.9b08347
ACS Nano 2020, 14, 2739−2750

bsIgG by controlled Fab arm exchange.[24] The resulting bsIgG retains its Fc-effector functions.[24]

Antibodies were generated and produced by expression in Expi293 (Thermo Fisher Scientific) as previously described.[35] Briefly, codon-optimized antibody genes encoding heavy and light chains were synthesized (GeneArt, Regensburg, Germany) and cloned separately into pcDNA3.3 (Thermo Fisher Scientific). All Fc domain mutations were introduced in heavy chain expression vectors either using QuikChange technology (Agilent Technologies, Santa Clara, CA) or *via* gene synthesis (GeneArt). The positions indicated represent numbers according to EU nomenclature. Antibodies were expressed in Expi293F cells by transfection of light chain and heavy chain expression vector DNA using ExpiFectamine 293 according to the manufacturer's instructions (Thermo Fisher Scientific). Antibodies were purified by Protein A affinity chromatography (rProtein A FF; GE Healthcare, Little Chalfont, Buckinghamshire, UK), dialyzed overnight against phosphate-buffered saline, and filter-sterilized over 0.2 μM dead-end filters (Corning, Amsterdam, The Netherlands). The concentration of purified IgG was determined by absorbance at 280 nm (Nanodrop photospectrometer, Thermo Scientific, Breda, The Netherlands) and by using the individually predicted extinction coefficient. Quality control of purified antibodies was performed by CE-SDS on the Labchip GXII (Caliper Life Sciences/PerkinElmer Hopkinton, MA, USA) under reducing and nonreducing conditions (>90% intact IgG, >95% HC + LC under reducing conditions), ESI-TOF MS (Waters, Hertfordshire, UK) or Orbitrap (Thermo Scientific), and HP-SEC (aggregate level <5%) (Waters Alliance 2975 separation unit, Waters) as described previously.[2]

Anti-DNP Fab fragments (IgG1-DNP-Fab) were generated from IgG1-DNP using the GingisKHAN Fab kit (Genovis, Lund, Sweden) according to the protocol supplied by the manufacturer.

Estimation of Local Concentrations, Rates, and Probabilities. Numeric values are based on estimates of the local concentrations c_1 and c_2 and the kinetic values determined in this study (Figures 2 and 3A). The local epitope/paratope concentrations c_i are given by

$$c_i = \frac{[\mathrm{epi}]A_i}{V_i N_A} \tag{3}$$

with V_i being the volume to which the unbound Fab is restricted, A_i being the corresponding surface area in which the Fab can reach an epitope, and N_A being Avogadro's number. In the state y_{1*} (Figure 4A) the unbound Fab arm can reach epitopes within a distance of 3–17 nm.[25] Modeling the respective volume/area as a hollow half-sphere/annulus with inner/outer radius of 3/17 nm and setting [epi] = 8.06 × 10^4 DNP epitopes/μm^2 (5 mol % DNP-cap-DPPE in the SLBs) thus yields a value of c_1 = 11.5 mM. The state y_2 (Figure 4A) features two unbound Fab fragments but occupies a higher volume and surface area, which we model as a half-sphere/circle with radius of 18 nm, yielding a value of c_2 = 15.4 mM. For estimation of $K_{D,Olig}$, we modeled the respective volume/area as a half-sphere/circle with a radius of 6 nm (~corresponding to the length of Fab/Fc fragments), yielding a value of c_{eff} = 33.5 mM.

Using these values we can calculate the probability P_i for a transition from state y_{1*} to y_1 and from state y_2 to y_{3*}, using

$$P_{y_{1*}\to y_1} = \frac{k_{on,Fab}c_1}{k_{off,Fab} + k_{on,Fab}c_1} \approx 1$$

, and

$$P_{y_2\to y_{3*}} = \frac{k_{on,Fab}c_2}{k_{off,Fc} + k_{on,Fab}c_2} \approx 0.18 \tag{4}$$

Note that the actual concentrations might differ from the estimated values as the model geometries differ from the actual ones. The IgG oligomerization propensity on a given antigenic surface with a given epitope concentration can thus be increased by either lowering $k_{off,Fc}$ through mutations that strengthen the Fc–Fc interaction or by increasing the local epitope/paratope concentrations, c_i, which can be achieved by optimizing the ratio A_i/V_i (eq 3), for instance through an optimization of the Fc fragment flexibility.

Detailed Model of IgG Oligomerization and Simulation of QCM Sensorgrams. We have deduced the system of rate equations governing the time course of the different IgG oligomer populations (y_1–y_{13}), the surface density of available epitopes (y_{14}), and the local concentration of IgGs close to the surface (y_{15})[27] for a given IgG concentration in the bulk solution C_{IgG} from the kinetic scheme given in Figure 4C. As an example of how the respective rate equations are obtained from the scheme, we briefly describe the terms contributing to the surface population of IgG monomers y_1 (first equation, below):

(1) Single IgGs in solution (concentration y_{15}) may bind to available surface epitopes (density y_{14}) with rate k_1 or dissociate from them with rate k_{-1} (first bracket).

(2) Following the vertical pathway, IgG monomers may transition into an incomplete dimer y_2 (were the Fab of the incoming IgG has not yet bound to a surface epitope) with forward rate k_2 and backward rate k_{-2} (second bracket).

(3) Following the lateral pathway, two epitope-bound monomers (y_1) may collide and form a dimer (y_3) with forward/backward rates k_6/k_{-6} (third bracket). The factor of 2 originates from the fact that always two monomers join to form a dimer/are released when a dimer dissociates.

(4) Accordingly, the next terms account for the formation/dissociation of a trimer (y_5) from/into a dimer (y_3) and a monomer (y_1) (fourth bracket; the factor of 2 in $2k_{-6}y_5$ accounts for two possibilities of how a trimer might dissociate into a dimer and a monomer),

5) the formation/dissociation of a tetramer (y_7) from/into a trimer (y_5) and a monomer (y_1) (fifth bracket; again a factor of 2 for two possibilities for the dissociation),

6) the formation/dissociation of a pentamer (y_9) from/into a tetramer (y_7) and a monomer (y_1) (sixth bracket; again a factor of 2 for two possibilities for the dissociation),

(7) the formation/dissociation of a hexamer with open Fc ring (y_{11}) from/into a pentamer (y_9) and a monomer (y_1) (seventh bracket; again a factor of 2 for two possibilities for the dissociation).

The complete set of corresponding rate equations reads

$$\frac{dy_1}{dt} = (k_1y_{14}y_{15} - k_{-1}y_1) - (k_2y_1y_{15} - k_{-2}y_2) - 2(k_6y_1(y_1 - 1) - k_{-6}y_3) - (k_6y_1y_3 - 2k_{-6}y_5) - (k_6y_1y_5 - 2k_{-6}y_7) - (k_6y_1y_7 - 2k_{-6}y_9) - (k_6y_1y_9 - 2k_{-6}y_{11})$$

$$\frac{dy_2}{dt} = k_2y_1y_{15} - k_{-2}y_2 - (k_3y_2y_{14} - 2k_{-1}y_3)$$

$$\frac{dy_3}{dt} = k_3y_{14}y_2 - 2k_{-1}y_3 - (k_2y_3y_{15} - k_{-2}y_4) + (k_6y_1(y_1 - 1) - k_{-6}y_3) - (k_6y_1y_3 - 2k_{-6}y_5)$$

$$\frac{dy_4}{dt} = k_2y_3y_{15} - k_{-2}y_4 - (k_4y_4y_{14} - 2k_{-1}y_5)$$

$$\frac{dy_5}{dt} = k_4y_{14}y_4 - 2k_{-1}y_5 - (k_2y_5y_{15} - k_{-2}y_6) + (k_6y_1y_3 - 2k_{-6}y_5) - (k_6y_1y_5 - 2k_{-6}y_7)$$

$$\frac{dy_6}{dt} = k_2y_5y_{15} - k_{-2}y_6 - (k_4y_6y_{14} - 2k_{-1}y_7)$$

https://dx.doi.org/10.1021/acsnano.9b08347
ACS Nano 2020, 14, 2739–2750

$$\frac{dy_7}{dt} = k_4 y_{14} y_6 - 2k_{-1} y_7 - (k_2 y_7 y_{15} - k_{-2} y_8) + (k_6 y_1 y_5 - 2k_{-6} y_7) - (k_6 y_1 y_7 - 2k_{-6} y_9)$$

$$\frac{dy_8}{dt} = k_2 y_7 y_{15} - k_{-2} y_8 - (k_4 y_8 y_{14} - 2k_{-1} y_9)$$

$$\frac{dy_9}{dt} = k_4 y_{14} y_8 - 2k_{-1} y_9 - (k_2 y_9 y_{15} - k_{-2} y_{10}) + (k_6 y_1 y_7 - 2k_{-6} y_9) - (k_6 y_1 y_9 - 2k_{-6} y_{11})$$

$$\frac{dy_{10}}{dt} = k_2 y_9 y_{15} - k_{-2} y_{10} - (k_4 y_{10} y_{14} - 2k_{-1} y_{11}) - (k_5 y_{10} - 2k_{-5} y_{12})$$

$$\frac{dy_{11}}{dt} = k_4 y_{10} y_{14} - 2k_{-1} y_{11} - (k_5 y_{11} - 6k_{-5} y_{13}) + k_6 y_1 y_9 - 2k_{-6} y_{11}$$

$$\frac{dy_{12}}{dt} = k_5 y_{10} - 2k_{-5} y_{12} - (k_4 y_{12} y_{14} - 6k_{-1} y_{13})$$

$$\frac{dy_{13}}{dt} = k_5 y_{11} - 6k_{-5} y_{13} + (k_4 y_{12} y_{14} - 6k_{-1} y_{13})$$

$$\frac{dy_{14}}{dt} = -w_1\left(\frac{dy_1}{dt} + \frac{dy_2}{dt}\right) - w_2\left(\frac{dy_3}{dt} + \frac{dy_4}{dt}\right) - w_3\left(\frac{dy_5}{dt} + \frac{dy_6}{dt}\right) - w_4\left(\frac{dy_7}{dt} + \frac{dy_8}{dt}\right) - w_5\left(\frac{dy_9}{dt} + \frac{dy_{10}}{dt}\right) - w_6\left(\frac{dy_{11}}{dt} + \frac{dy_{12}}{dt} + \frac{dy_{13}}{dt}\right)$$

$$\frac{dy_{15}}{dt} = k_{tr}(C_{IgG} - y_{15}) - (k_1 y_{14} y_{15} - k_{-1} y_1 + k_2 y_1 y_{15} - k_{-2} y_2 + k_2 y_3 y_{15} - k_{-2} y_4 + k_2 y_5 y_{15} - k_{-2} y_6 + k_2 y_7 y_{15} - k_{-2} y_8 + k_2 y_9 y_{15} - k_{-2} y_{10}) \quad (5)$$

We implemented a two-compartment model[27] that accounts for potential mass transport effects (rate k_{tr}) between regions close to the surface with IgG concentration y_{15} and regions far from the surface where the IgG concentration is that of the bulk, C_{IgG}. The constants k_i and k_{-i} are the forward and backward rates associated with the transitions between the different oligomer configurations: k_1, k_{-1}, k_2, and k_{-2} are given by $k_{on,Fab}$, $k_{off,Fab}$, $4k_{on,Fc}$, and $k_{off,Fc}$. The transition rate from state y_2 to y_3 is given by $k_3 = k_{on,Fab}c_3$ and differs from $k_4 = k_{on,Fab}c_4$ as the respective geometries (eq 3) differ (single attachment to the surface and associated flexibility in state y_2 *vs* multiple attachments in states y_4, y_6, y_8, *etc.*). k_5 and k_{-5} are the forward and backward rates of Fc ring stabilization, and k_6 and k_{-6} account for the oligomerization through lateral collisions between IgG monomers and other oligomers. The parameters w_i account for epitopes (surface density [epi]) that are unbound but also unavailable as they are screened by (hidden below) other IgGs bound to neighboring epitopes and are given by

$$w_1 = \frac{d_1^2\pi}{4}[\text{epi}]$$

$$w_{n=2...5} = \left(\frac{n}{6}\frac{d_2^2\pi}{4} + d_2\Delta\right)[\text{epi}]$$

$$w_6 = \frac{(d_2)^2\pi}{4}[\text{epi}] \quad (6)$$

A single monovalent IgG screens a circular patch of diameter d_1 = 8.8 nm,[36] hexamers screen a circular patch of diameter d_2 = 23 nm,[34] and dimers to pentamers screen the respective fragment of a hexamer plus an additional area ($d_2\Delta$, with Δ = 2.9 nm) accounting for overlap effects at the rim (along the Fc portions) of these oligomers.

We numerically solved the system of rate equations (eq 5) using the kinetic rates obtained from SMFS and QCM experiments (Figures 2 and 3) and adjusting the unknown rates (Table 1) to reproduce the experimental QCM sensorgrams (C_{IgG} = 133 nM) for monovalent IgGs as shown in Figure 3B. Since the QCM detects the sum of all molecules bound to the sensor chip, the respective oligomer surface densities had to be weighted by their respective oligomeric state (*i.e.*, a hexamer contributes 6× the signal of a monomer to the sensorgram, *etc.*). For the initial association phase we used initial conditions $y_{0,i} = 0$ for $i \neq 14$ and $y_{0,14} = 8.06 \times 10^4$ DNP epitopes/μm^2 (corresponding to 5 mol % DNP-cap-DPPE in the SLBs). The dissociation phase was simulated by setting $C_{IgG} = 0$ after the association phase.

ASSOCIATED CONTENT

Supporting Information

The Supporting Information is available free of charge at https://pubs.acs.org/doi/10.1021/acsnano.9b08347.

HS-AFM images and oligomer abundance histograms demonstrating a mutation-induced reduction of IgG oligomerization; influence of antigen specificity on oligomer abundance (PDF)

AUTHOR INFORMATION

Corresponding Author

Johannes Preiner − *University of Applied Sciences Upper Austria, Linz, Austria;* orcid.org/0000-0002-6755-6543; Email: johannes.preiner@fh-linz.at

Other Authors

Jürgen Strasser − *University of Applied Sciences Upper Austria, Linz, Austria*

Rob N. de Jong − *Genmab, Utrecht, The Netherlands*

Frank J. Beurskens − *Genmab, Utrecht, The Netherlands*

Janine Schuurman − *Genmab, Utrecht, The Netherlands*

Paul W. H. I. Parren − *Leiden University Medical Center, Leiden, The Netherlands, and Lava Therapeutics, Utrecht, The Netherlands*

Peter Hinterdorfer − *Johannes Kepler University Linz, Linz, Austria;* orcid.org/0000-0003-2583-1305

Complete contact information is available at: https://pubs.acs.org/10.1021/acsnano.9b08347

Author Contributions

F.J.B., J.P., Ja.S., P.H., R.N.d.J., and P.W.H.I.P conceived the project. J.P. and J.S. analyzed the data. F.J.B., J.P., J.S., R.N.d.J., and P.W.H.I.P. wrote the manuscript. All authors commented on the manuscript. J.P. and J.S. designed SMFS, HS-AFM, and QCM experiments. J.S. performed HS-AFM, SMFS, and QCM. J.P. developed the model and performed simulations.

Notes

The authors declare the following competing financial interest(s): F.J.B., R.N.d.J., Ja.S., and P.W.H.I.P. are inventors on patent applications related to complement activation by therapeutic antibodies and own Genmab stock. J.S. and J.P. received Genmab funding.

https://dx.doi.org/10.1021/acsnano.9b08347
ACS Nano 2020, 14, 2739−2750

ACKNOWLEDGMENTS

We gratefully acknowledge technical support from A. Ebner (JKU Linz, Austria) and F. Kienberger (Keysight, Austria). This work was supported by the European Fund for Regional Development (EFRE, IWB2020), the Federal State of Upper Austria, and the Austrian Science Fund (FWF, P25844 to J.P.).

REFERENCES

(1) Diebolder, C. A.; Beurskens, F. J.; de Jong, R. N.; Koning, R. I.; Strumane, K.; Lindorfer, M. A.; Voorhorst, M.; Ugurlar, D.; Rosati, S.; Heck, A. J. R.; van de Winkel, J. G. J.; Wilson, I. A.; Koster, A. J.; Taylor, R. P.; Saphire, E. O.; Burton, D. R.; Schuurman, J.; Gros, P.; Parren, P. W. H. I. Complement Is Activated by IgG Hexamers Assembled at the Cell Surface. *Science* **2014**, *343*, 1260−1263.

(2) de Jong, R. N.; Beurskens, F. J.; Verploegen, S.; Strumane, K.; van Kampen, M. D.; Voorhorst, M.; Horstman, W.; Engelberts, P. J.; Oostindie, S. C.; Wang, G.; Heck, A. J. R.; Schuurman, J.; Parren, P. W. H. I. A Novel Platform for the Potentiation of Therapeutic Antibodies Based on Antigen-Dependent Formation of IgG Hexamers at the Cell Surface. *PLoS Biol.* **2016**, *14*, No. e1002344.

(3) van der Horst, H. J.; Overdijk, M. B.; Breij, E. C.; Chamuleau, M.; Lokhorst, H. M.; Mutis, T. Potent *Ex Vivo* Anti-Tumor Activity in Relapsed Refractory Multiple Myeloma Using Novel DR5-Specific Antibodies with Enhanced Capacity to Form Hexamers upon Target Binding. *Blood* **2017**, *130*, 1835−1835.

(4) Oostindie, S. C.; van derHorst, H. J.; Lindorfer, M. A.; Cook, E. M.; Tupitza, J. C.; Zent, C. S.; Burack, R.; VanDerMeid, K. R.; Strumane, K.; Chamuleau, M. E. D.; Mutis, T.; de Jong, R. N.; Schuurman, J.; Breij, E. C. W.; Beurskens, F. J.; Parren, P. W. H. I.; Taylor, R. P. CD20 and CD37 Antibodies Synergize to Activate Complement by Fc-Mediated Clustering. *Haematologica* **2019**, *104*, 1841.

(5) Zhang, D.; Goldberg, M. V.; Chiu, M. L. Fc Engineering Approaches to Enhance the Agonism and Effector Functions of an Anti-OX40 Antibody. *J. Biol. Chem.* **2016**, *291*, 27134−27146.

(6) Overdijk, M. B.; Strumane, K.; Buijsse, A. O.; Vermot-Desroches, C.; Kroes, T.; Jong, B. de; Hoevenaars, N.; Beurskens, F. J.; Jong, R. N. de; Lingnau, A.; Parren, P. W.; Forssmann, U.; Sasser, A. K.; Schuurman, J.; Breij, E. C. Abstract 2391: DR5 Agonist Activity of HexaBody®-DR5/DR5 (GEN1029) Is Potentiated by C1q and Independent of Fc-Gamma Receptor Binding in Preclinical Tumor Models. *Cancer Res.* **2019**, *79*, 2391−2391.

(7) Zhang, D.; Armstrong, A. A.; Tam, S. H.; McCarthy, S. G.; Luo, J.; Gilliland, G. L.; Chiu, M. L. Functional Optimization of Agonistic Antibodies to OX40 Receptor with Novel Fc Mutations to Promote Antibody Multimerization. *mAbs* **2017**, *9*, 1129−1142.

(8) Strasser, J.; de Jong, R. N.; Beurskens, F. J.; Wang, G.; Heck, A. J. R.; Schuurman, J.; Parren, P. W. H. I.; Hinterdorfer, P.; Preiner, J. Unraveling the Macromolecular Pathways of IgG Oligomerization and Complement Activation on Antigenic Surfaces. *Nano Lett.* **2019**, *19*, 4787−4796.

(9) Wang, G.; de Jong, R. N.; van den Bremer, E. T. J.; Beurskens, F. J.; Labrijn, A. F.; Ugurlar, D.; Gros, P.; Schuurman, J.; Parren, P. W. H. I.; Heck, A. J. R. Molecular Basis of Assembly and Activation of Complement Component C1 in Complex with Immunoglobulin G1 and Antigen. *Mol. Cell* **2016**, *63*, 135−145.

(10) Ando, T.; Kodera, N.; Takai, E.; Maruyama, D.; Saito, K.; Toda, A. A High-Speed Atomic Force Microscope for Studying Biological Macromolecules. *Proc. Natl. Acad. Sci. U. S. A.* **2001**, *98*, 12468−12472.

(11) Preiner, J.; Kodera, N.; Tang, J.; Ebner, A.; Brameshuber, M.; Blaas, D.; Gelbmann, N.; Gruber, H. J.; Ando, T.; Hinterdorfer, P. IgGs Are Made for Walking on Bacterial and Viral Surfaces. *Nat. Commun.* **2014**, *5*, DOI: 10.1038/ncomms5394.

(12) Preiner, J.; Horner, A.; Karner, A.; Ollinger, N.; Siligan, C.; Pohl, P.; Hinterdorfer, P. High-Speed AFM Images of Thermal Motion Provide Stiffness Map of Interfacial Membrane Protein Moieties. *Nano Lett.* **2015**, *15*, 759−763.

(13) Karner, A.; Nimmervoll, B.; Plochberger, B.; Klotzsch, E.; Horner, A.; Knyazev, D. G.; Kuttner, R.; Winkler, K.; Winter, L.; Siligan, C.; Ollinger, N.; Pohl, P.; Preiner, J. Tuning Membrane Protein Mobility by Confinement into Nanodomains. *Nat. Nanotechnol.* **2017**, *12*, 260−266.

(14) Evans, E.; Ritchie, K. Dynamic Strength of Molecular Adhesion Bonds. *Biophys. J.* **1997**, *72*, 1541−1555.

(15) Keiji Kanazawa, K.; Gordon, J. G. The Oscillation Frequency of a Quartz Resonator in Contact with Liquid. *Anal. Chim. Acta* **1985**, *175*, 99−105.

(16) Kasper, M.; Traxler, L.; Salopek, J.; Grabmayr, H.; Ebner, A.; Kienberger, F. Broadband 120 MHz Impedance Quartz Crystal Microbalance (QCM) with Calibrated Resistance and Quantitative Dissipation for Biosensing Measurements at Higher Harmonic Frequencies. *Biosensors* **2016**, *6*, 23.

(17) Friddle, R. W.; Noy, A.; De Yoreo, J. J. Interpreting the Widespread Nonlinear Force Spectra of Intermolecular Bonds. *Proc. Natl. Acad. Sci. U. S. A.* **2012**, *109*, 13573−13578.

(18) Hinterdorfer, P.; Baumgartner, W.; Gruber, H. J.; Schilcher, K.; Schindler, H. Detection and Localization of Individual Antibody-Antigen Recognition Events by Atomic Force Microscopy. *Proc. Natl. Acad. Sci. U. S. A.* **1996**, *93*, 3477−3481.

(19) Zhu, R.; Howorka, S.; Pröll, J.; Kienberger, F.; Preiner, J.; Hesse, J.; Ebner, A.; Pastushenko, V. P.; Gruber, H. J.; Hinterdorfer, P. Nanomechanical Recognition Measurements of Individual DNA Molecules Reveal Epigenetic Methylation Patterns. *Nat. Nanotechnol.* **2010**, *5*, 788−791.

(20) Rankl, C.; Kienberger, F.; Wildling, L.; Wruss, J.; Gruber, H. J.; Blaas, D.; Hinterdorfer, P. Multiple Receptors Involved in Human Rhinovirus Attachment to Live Cells. *Proc. Natl. Acad. Sci. U. S. A.* **2008**, *105*, 17778.

(21) DeLano, W. L.; Ultsch, M. H.; De, A. M.; Vos; Wells, J. A. Convergent Solutions to Binding at a Protein-Protein Interface. *Science* **2000**, *287*, 1279−1283.

(22) Hamilton, R. G. Human IgG Subclass Measurements in the Clinical Laboratory. *Clin. Chem.* **1987**, *33*, 1707−1725.

(23) Vidarsson, G.; Dekkers, G.; Rispens, T. IgG Subclasses and Allotypes: From Structure to Effector Functions. *Front. Immunol.* **2014**, *5*, DOI: 10.3389/fimmu.2014.00520.

(24) Labrijn, A. F.; Meesters, J. I.; de Goeij, B. E.; van den Bremer, E. T.; Neijssen, J.; van Kampen, M. D.; Strumane, K.; Verploegen, S.; Kundu, A.; Gramer, M. J.; van Berkel, P. H. C.; van de Winkel, J. G. J.; Schuurman, J.; Parren, W. H. I. Efficient Generation of Stable Bispecific IgG1 by Controlled Fab-Arm Exchange. *Proc. Natl. Acad. Sci. U. S. A.* **2013**, *110*, 5145−5150.

(25) Shaw, A.; Hoffecker, I. T.; Smyrlaki, I.; Rosa, J.; Grevys, A.; Bratlie, D.; Sandlie, I.; Michaelsen, T. E.; Andersen, J. T.; Högberg, B. Binding to Nanopatterned Antigens Is Dominated by the Spatial Tolerance of Antibodies. *Nat. Nanotechnol.* **2019**, *1*, 184−190.

(26) Kane, R. S. Thermodynamics of Multivalent Interactions: Influence of the Linker. *Langmuir* **2010**, *26*, 8636−8640.

(27) Schuck, P.; Zhao, H. The Role of Mass Transport Limitation and Surface Heterogeneity in the Biophysical Characterization of Macromolecular Binding Processes by SPR Biosensing. In *Surface Plasmon Resonance*; Methods in Molecular Biology; Mol, N., Fischer, M., Eds.; Humana Press: New York, 2010; pp 15−54.

(28) Burton, D. R.; Pyati, J.; Koduri, R.; Sharp, S. J.; Thornton, G. B.; Parren, P. W.; Sawyer, L. S.; Hendry, R. M.; Dunlop, N.; Nara, P. L.; Et, A. Efficient Neutralization of Primary Isolates of HIV-1 by a Recombinant Human Monoclonal Antibody. *Science* **1994**, *266*, 1024−1027.

(29) Ebner, A.; Wildling, L.; Zhu, R.; Rankl, C.; Haselgrubler, T.; Hinterdorfer, P.; Gruber, H. J. Functionalization of Probe Tips and Supports for Single Molecule Recognition Force Microscopy. *Top. Curr. Chem.* **2008**, *285*, 29−76.

(30) Sauerbrey, G. Verwendung von Schwingquarzen zur Wägung dünner Schichten und zur Mikrowägung. *Eur. Phys. J. A* **1959**, *155*, 206−222.

https://dx.doi.org/10.1021/acsnano.9b08347
ACS Nano 2020, 14, 2739−2750

(31) Höök, F.; Vörös, J.; Rodahl, M.; Kurrat, R.; Böni, P.; Ramsden, J. J.; Textor, M.; Spencer, N. D.; Tengvall, P.; Gold, J.; Kasemo, B. A Comparative Study of Protein Adsorption on Titanium Oxide Surfaces Using *In Situ* Ellipsometry, Optical Waveguide Lightmode Spectroscopy, and Quartz Crystal Microbalance/Dissipation. *Colloids Surf., B* **2002**, *24*, 155−170.
(32) Leekumjorn, S.; Sum, A. K. Molecular Simulation Study of Structural and Dynamic Properties of Mixed DPPC/DPPE Bilayers. *Biophys. J.* **2006**, *90*, 3951−3965.
(33) White, K. D.; Frank, M. B.; Foundling, S.; Waxman, F. J. Effect of Immunoglobulin Variable Region Structure on C3b and C4b Deposition. *Mol. Immunol.* **1996**, *33*, 759−768.
(34) Ugurlar, D.; Howes, S. C.; de Kreuk, B.-J.; Koning, R. I.; de Jong, R. N.; Beurskens, F. J.; Schuurman, J.; Koster, A. J.; Sharp, T. H.; Parren, P. W. H. I.; Gros, P. Structures of C1-IgG1 Provide Insights into How Danger Pattern Recognition Activates Complement. *Science* **2018**, *359*, 794−797.
(35) Vink, T.; Oudshoorn-Dickmann, M.; Roza, M.; Reitsma, J.-J.; de Jong, R. N. A Simple, Robust and Highly Efficient Transient Expression System for Producing Antibodies. *Methods* **2014**, *65*, 5−10.
(36) Michele, C. D.; Rios, P. D. L.; Foffi, G.; Piazza, F. Simulation and Theory of Antibody Binding to Crowded Antigen-Covered Surfaces. *PLoS Comput. Biol.* **2016**, *12*, No. e1004752.
(37) Saphire, E. O.; Parren, P. W. H. I.; Pantophlet, R.; Zwick, M. B.; Morris, G. M.; Rudd, P. M.; Dwek, R. A.; Stanfield, R. L.; Burton, D. R.; Wilson, I. A. Crystal Structure of a Neutralizing Human IgG Against HIV-1: A Template for Vaccine Design. *Science* **2001**, *293*, 1155−1159.

https://dx.doi.org/10.1021/acsnano.9b08347
ACS Nano 2020, 14, 2739−2750